Earth Surface Processes and Landforms
Earth Surf. Process. Landforms **30**, 1547–1566 (2005)
Published online 26 August 2005 in Wiley InterScience (www.interscience.wiley.com). **DOI:** 10.1002/esp.1212

Modelling water erosion in the Sahel: application of a physically based soil erosion model in a gentle sloping environment

S. M. Visser[1]*, G. Sterk[1] and D. Karssenberg[2]

[1] *Department of Environmental Sciences, Erosion & Soil and Water Conservation Group, Wageningen University. Nieuwe Kanaal 11, 6908 PA Wageningen, The Netherlands*

[2] *The Netherlands Centre for Geo-ecological Research (ICG), Faculty of Geographical Sciences, Utrecht University, PO Box 80115, 3508 TC Utrecht, The Netherlands*

**Correspondence to: S. M. Visser, Department of Environmental Sciences, Erosion & Soil and Water Conservation Group, Wageningen University. Nieuwe Kanaal 11, 6908 PA Wageningen, The Netherlands. E-mail: Saskia.Faye-Visser@wur.nl*

Received 25 July 2003;
Revised 19 October 2004;
Accepted 23 November 2004

Abstract

Water is a major limiting factor in arid and semi-arid agriculture. In the Sahelian zone of Africa, it is not always the limited amount of annual rainfall that constrains crop production, but rather the proportion of rainfall that enters the root zone and becomes plant-available soil moisture. Maximizing the rain-use efficiency and therefore limiting overland flow is an important issue for farmers. The objectives of this research were to model the processes of infiltration, runoff and subsequent erosion in a Sahelian environment and to study the spatial distribution of overland flow and soil erosion.

The wide variety of existing water erosion models are not developed for the Sahel and so do not include the unique Sahelian processes. The topography of the Sahelian agricultural lands in northern Burkina Faso is such that field slopes are generally low (0–5°) and overland flow mostly occurs in the form of sheet flow, which may transport large amounts of fine, nutrient-rich particles despite its low sediment transport capacity. Furthermore, pool formation in a field limits overland flow and causes resettlement of sediment resulting in the development of a surface crust.

The EUROSEM model was rewritten in the dynamic modelling code of PCRaster and extended to account for the pool formation and crust development. The modelling results were calibrated with field data from the 2001 rainy season in the Katacheri catchment in northern Burkina Faso. It is concluded that the modified version of EUROSEM for the Sahel is a fully dynamic erosion model, able to simulate infiltration, runoff routing, pool formation, sediment transport, and erosion and deposition by inter-rill processes over the land surface in individual storms at the scale of both runoff plots and fields. A good agreement is obtained between simulated and measured amounts of runoff and sediment discharge. Incorporating crust development during the event may enhance model performance, since the process has a large influence on infiltration capacity and sediment detachment in the Sahel. Copyright © 2005 John Wiley & Sons, Ltd.

Keywords: Sahel; Burkina Faso; water erosion; physically-based erosion model; PCRaster

Introduction

Approximately 90 per cent of the population in the Sahelian zone of Burkina Faso lives from self-sustaining agriculture (Thiombiano, 2000). The sedentary farmers often combine animal husbandry with rain-fed crop production. Rapid population growth has resulted in the expansion of the cropped area onto more marginal land, which was previously used as communal grazing land. Consequently, larger areas are stripped of their vegetation and left bare and vulnerable for erosion by both wind and water in the early rainy season.

The Sahelian soils, which generally have a sandy to sandy loam texture, are characterized by a low organic matter content and low soil fertility. Furthermore the soils are prone to crusting and have low water-holding capacities

(Valentin, 1995). In addition the climatic conditions are harsh and rainfall is highly variable both within the year and between years. The combination of the highly variable rain, the high temperatures, a potential evapotranspiration exceeding precipitation for most of the year, and poor soils make agricultural crop production difficult (Sterk, 2003).

Although water is a major limiting factor in the Sahel (Lal, 1988), it is not always the amount of rainfall, but the proportion of rainfall that becomes plant-available soil moisture that limits crop production (Sivakumar and Wallance, 1991). Due to crust formation, which significantly decreases infiltration rates, large amounts of rainfall are lost in the form of overland flow (generally sheet flow) and evapotranspiration (in the case of stagnating water). Apart from carrying away valuable water, once overland flow is generated it causes erosion and is the transporting agent for dislodged soil particles and plant nutrients; overland flow also results in the degradation of the nutrient content of the topsoil (Guy *et al*., 1987). Furthermore, overland flow may cause direct damage to the crop. Young plants are damaged by the effect of flowing water and plants die from the effects of stagnating water: both processes result in reduced yields (Veihe, 2000). Hence, conservation tools to limit overland flow generation and water erosion are necessary.

In order to use soil and water conservation tools effectively or to develop new tools for water erosion control, a good insight into the erosion processes is necessary. A process-based water erosion model developed for the Sahelian situation would be a useful tool in the battle against erosion since it gives insight to the interaction of the various controlling processes. Furthermore, such a model could predict erosion risk under various land management practices.

Present water erosion models are mostly developed for application on sloping areas in modern western agricultural systems. Whereas these models include specific processes such as the limited infiltration in wheel tracks, they lack the specific Sahelian processes. First of all, large cultivated areas in the Sahel have low slopes but are subjected to water erosion. Specific water erosion processes, such as rill and gully formation, do not occur but overland flow occurs in the form of a turbulent sheet flow. The transport capacity of this flow is increased by the impact of wind-driven rainfall. Hence sheet flow in this area can transport large amounts of fine, but nutrient-rich particles.

Due to the low topographic differences, pool formation occurs resulting in, on the one hand, reduced overland flow discharge, but on the other hand the death of crops due to stagnating water and crust development. Crust development in the Sahel has large influences on infiltration rate and sediment availability. Therefore preferably crust development, but at least the spatial distribution of crust types in the field, should be incorporated in a Sahelian water erosion model. Furthermore, pool formation traps large amounts of water and sediment, limiting total runoff. This process should be incorporated in a water erosion model applied in the Sahel.

The present study aims to develop a physically based model that incorporates all water erosion controlling processes in a Sahelian environment. The model is calibrated and tested with field data from the 2001 rainy season in the Katacheri catchment in northern Burkina Faso.

Materials and Methods

General structure of the model

The European Soil Erosion Model (EUROSEM) (Morgan, 1995; Morgan *et al*., 1992) was rewritten to make it applicable for the Sahelian situation. EUROSEM was previously applied outside Europe, and though the model needed calibration for individual catchments, the results were promising (Veihe *et al*., 2001).

EUROSEM is the result of a collaborative research programme involving scientists from ten European countries and the USA. Considering that erosion is dominated by only a few events per year, which are characterized by a highly dynamic behaviour, EUROSEM is developed as an event-based model designed to operate for successive short (e.g. one minute) time steps within a storm. The model simulates erosion on a single plane or segment. Each segment is assumed to have uniform properties. Linking various segments with different properties accounts for the spatial variability in input parameters at a hill slope. By joining these hill slopes with channel elements, small catchments can be represented.

EUROSEM has a modular structure (Figure 1), which makes it easy to replace and/or adapt several modules. The grey boxes in Figure 1 indicate the modules that are adapted for Sahelian environments. Most of the key equations of the model are given in Table I. EUROSEM deals with the interception of rainfall by the plant cover; the volume of rainfall that reaches the ground directly through fall and leaf drainage; the volume of depression storage; the detachment of the soil by rainfall and overland flow; the transport capacity of the overland flow; and the deposition of sediment (Figure 1, Table I). Overland flow is routed over the soil surface using the kinematic wave equation (Equation III, Table I). Soil loss is computed as a sediment discharge, defined as the product of the volume of overland

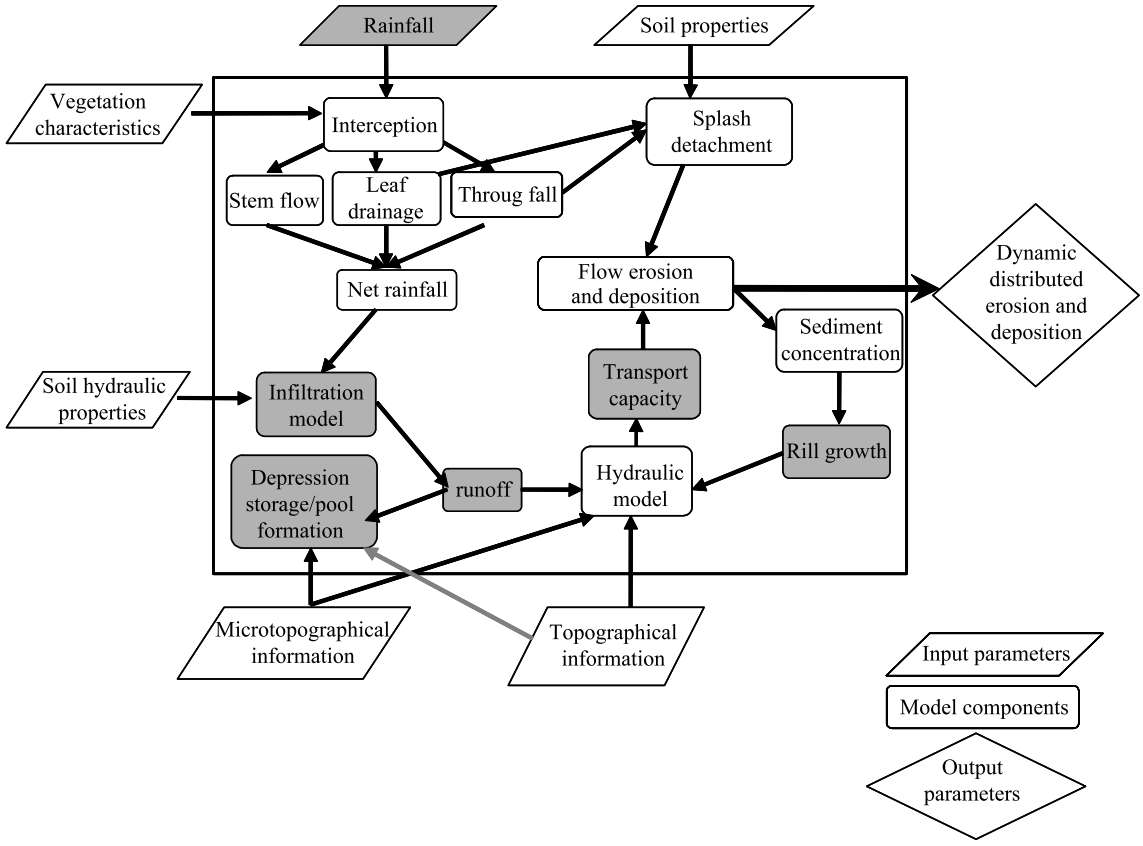

Figure 1. Flow chart of the European Soil Erosion Model (EUROSEM) (Morgan *et al.*, 1992). Grey boxes indicate the modules that are adapted for Sahelian environments.

flow and the sediment concentration in the flow, to give a volume of sediment passing a given point in a given time period. The computation is based on the dynamic mass balance equation (Equation IX, Table I). Soil erodibility is represented through the use of soil cohesion and an index expressing its detachability by raindrop impact. Rill and inter-rill processes are modelled explicitly with water and sediment routed from the inter-rill to the rill area. Vegetation or crop cover are incorporated into the model by their effect on the volume and energy of the rain reaching the ground surface, infiltration, roughness imparted to the flow, and reinforcement of soil cohesion by the root system. By describing the soil, microtopography and vegetation conditions associated with each soil conservation practice, soil conservation measures can be simulated.

Adaptation for the Sahel

The EUROSEM modules for precipitation, infiltration and overland flow routing were adapted for the Sahelian situation. A pool formation module is also added to the model. These adaptations will be discussed in the following sections. The PCRaster version of EUROSEM (Van Dijck and Karssenberg, 2000) was used in this study. This version of EUROSEM differs from the original version mainly in that it is raster based and written in the environmental modelling language PCRaster (De Jong, 1997). The version used included only the water components of EUROSEM, but was extended here with the erosion components based on the work of Van der Perk and Slavik (2003). One of the main advantages of incorporating EUROSEM in PCRaster is the relatively open data structure of PCRaster, which allows the model builder to closely follow the erosion simulation and to make model adaptations relatively easily. Due to its physical character the model requires a large number of input parameters. Table II shows all input parameters required for the model application in the Sahel and the measurement methods. In the following sections the main adaptations of the model and the field measurements are discussed.

Table I. Operating equations of the European Soil Erosion Model as used in this research (for brevity some equations have been excluded)

No.	Model subroutine and key equation	Definition of terms	Source
I	Interception: $I_c = RP_c$	R, depth of rainfall (mm); P_c, percentage of canopy cover expressed as a ratio	Merriam (1973)
II	Interception storage: $I_{cs} = I_x(1 - e^{(R_c - I_x)})$	I_{cs}, interception storage (mm), R_c, cumulative rainfall (mm), I_x, maximum interception storage (mm)	Van Elewijck (1989)
III	Surface runoff continuity: $q_{(x,t)} = \left(\frac{\delta h}{\delta t}\right) - \left(\frac{\delta Q}{\delta x}\right)$	$q_{(x,t)}$, lateral inflow rate ($m^3 s^{-1}$), t, time step (s)	Woolhiser *et al.* (1990)
IV	Soil detachment by rain: $D_s = kK_e e^{-bh}$	k, detachability of the soil ($g J^{-1}$), K_e, kinetic energy of the rain ($J m^{-1}$ per mm of rainfall); b, exponent (1 to 3); h, water depth at the soil surface (m)	Brandt (1989)
V	Kinetic energy leaf drainage: $K_e(LD) = (15{\cdot}8P_h^{0{\cdot}5}) - 5{\cdot}87$	$K_e(LD)$, kinetic energy ($J m^{-2}$ per mm of leaf drainage); P_h, height of the plant canopy (m)	Brandt (1989)
VI	Soil detachment by flow: $D_F = \beta\Omega v_s(C_m - C)$	C_m, equilibrium sediment concentration in the flow ($g m^{-3}$); C, actual sediment concentration ($g m^{-3}$); β, resistance of the soil to detachment (kPa); Ω, stream power ($g cm^{-1} s^{-1}$); v_s, settling velocity of the soil particle ($m s^{-1}$)	Smith *et al.* (1995)
VII	where $\Omega = uS$	u, mean flow velocity ($cm s^{-1}$); S, slope (deg)	Govers (1990)
VIII	$TC = \frac{b}{\rho_s q}((\Omega - \Omega_c)^{0{\cdot}7/n} - 1)^n$	TC, transport capacity ($kg m^{-3}$); b, function of particle size (m); Ω, stream power ($g cm^{-1} s^{-1}$); Ω_c, effective stream power ($g cm^{-1} s^{-1}$), n, 5	Morgan *et al.* (1992)
IX	Sediment continuity: $q_s(x, t) = \frac{\delta(AC)}{\delta t} + \frac{\delta(AC)}{\delta t} - e(x, t)$	q_s, lateral input or extraction of sediment per unit length of flow ($m^3 s^{-1}$); A, cross-sectional area of the flow (m^2); Q, discharge ($m^3 s^{-1}$); e, net pickup rate of sediment from the bed per unit length of flow ($m^3 s^{-1}$); x, horizontal distance (m)	Bennet (1974); Kirkby (1980); Woolhiser *et al.* (1990)

Rainfall

In the early rainy season in the Sahel, rainfall comes with heavy thunderstorms that move westward through the Sahel. The vegetation of the arable land can be classified as a parkland system (trees and shrubs scattered amongst crops) which is characterized by an open structure. So winds are not much hindered by vegetation. As a result of the strong winds the raindrops have a significant horizontal velocity, which increases their resultant impact velocity (Umback and Lembke, 1966). Furthermore, the distribution and intensity of rain on sloping surfaces changes according to wind direction and velocity.

Simple geometric relations were used to express the relation between the amount of water falling intercepted in a rain gauge and the amount of water reaching the soil surface (Figure 2). The amount of water intercepted by a horizontally positioned rain gauge depends, besides i (angle of incidence, in degrees), on the area X (m^2) of the gauge with diameter d_0 (m) (Figure 2A and B). When rain reaches the gauge with an angle $i \neq 0$, the effective area changes and the cross-section of the column of rain intercepted by the gauge is elliptical, with area $Xcos(i)$. Hence the real rainfall intensity R ($m h^{-1}$) is related to the intensity intercepted by the gauge by (Sharon, 1980):

$$R = \frac{I}{\cos(i)} \tag{1}$$

where R is the intensity of rainfall in respect to a plane normal to the storm vector ($m h^{-1}$) and I is the intensity of rainfall measured with a horizontally placed gauge ($m h^{-1}$).

In the case of a sloping surface, rain intensity can become higher or lower, depending on the slope aspect with respect to the wind direction (Figure 2C and D). Hence the intensity at the slope surface is:

$$I_s = R\cos(i \pm \alpha) \tag{2}$$

Table II. Parameters and input variables of the adapted EUROSEM model and measurement methods

Parameter	Description	Method	Reference
DEM	Digital Elevation Model (m)	Height measured with a level in a 2 × 2 grid	
Crust	Map with the distribution of soil crusts	Description of crust type in two transects and at 17 fixed positions in the research site	Valentin and Bresson (1992)
LDD	Map with local drain direction	Calculated by PCRaster based on DEM and pool position*	De Jong (1997)
Rain	Table with rainfall per minute (mm)	Field measurements with tipping bucket	
Wind Speed	Table with wind speed per minute (m s^{-1})	Field measurement with Vector wind anenometer	
Wind Dir	Table with wind direction per minute (deg)	Field measurement with Vector wind vane	
K_e	Saturated conductivity (cm h^{-1})	Based on rainfall simulations and crust development	Horstman (2003)
ψ	Wetting front suction head (cm)	Literature	Chow *et al.* (1988)
θ_k	Residual moisture content	PF-curve/literature	Chow *et al.* (1988)
θ_e	Effective porosity	PF-curve/literature	Chow *et al.* (1988)
θ_i	Initial moisture content	Field measurements with theta probe	
Cover	Map with fractions of surface coverage by vegetation	1-m^2 square with wire mesh at 10 cm intervals, measurements made at 17 points in the research plot	Morgan *et al.* (1992)
LAI	Map with leaf area index	Based on cover map and literature	Morgan *et al.* (1992)
Crop Height	Average crop height (m)	Measured in the field with regular time intervals	
Pool Map	Various maps for prediction of pool formation	Based on DEM*	
SLRR	Random roughness	Saleh's chain method	Saleh (1993)
N	Manning's *N*	Literature	Morgan *et al.* (1992)
k	Index of soil detachability	Splash cups	Poesen (1985)
D_{50}	Median grain size (cm)		
ρ_s	Particle density (kg m^{-3})	Literature	Kutilek and Nielsen (1994)
ρ_w	Water density (kg m^{-3})	Literature	Kutilek and Nielsen (1994)
Coh	Table with cohesion values of bare crust (kPa)	Thorvane measurements over the season	Morgan *et al.* (1992)
AddCoh	Map with additional cohesion by vegetation roots	Based on cover map and literature	Morgan *et al.* (1992)

* See 'Pool formation' section

where I_s is the rain intensity at the soil surface (m h^{-1}) and α is slope (degrees).

To determine the angle of incidence the following equation was used (Sharon, 1980):

$$i = -0{\cdot}2070\sqrt{\bar{u}} + 7{\cdot}1378\bar{u} \tag{3}$$

where $\bar{u}$ is wind speed (m s^{-1}).

The kinetic energy of a raindrop hitting the soil surface is an important parameter in determining the amount of splash detachment. A raindrop hitting the soil surface at an angle will exert a different energy on the soil surface from a raindrop hitting the soil surface from the vertical. The kinetic energy (J m^{-2} per mm of rainfall) of the wind-driven rain directly reaching the soil surface (direct through fall in EUROSEM) is given by (Pedersen and Hasholt, 1995):

$$KE = \gamma_1 e^{\beta_1 \bar{u}} \ln(I) + \gamma_2 e^{\beta_2 \bar{u}} \tag{4}$$

where γ_1 is 5·27, γ_2 is 10·61, β_1 is 0·07 and β_2 is 0·12.

Infiltration

The formation of a seal or crust at the soil surface alters the way water is partitioned at the surface, resulting in decreased infiltration and increased overland flow and erosion (Bristow *et al.*, 1994). The reduction depends upon the soil type, surface conditions and the rainfall's kinetic energy, intensity and duration. Even very sandy soils (90 per cent sand) can experience reduced infiltration due to crust formation (Hoogmoed and Stroosnijder, 1984). Despite

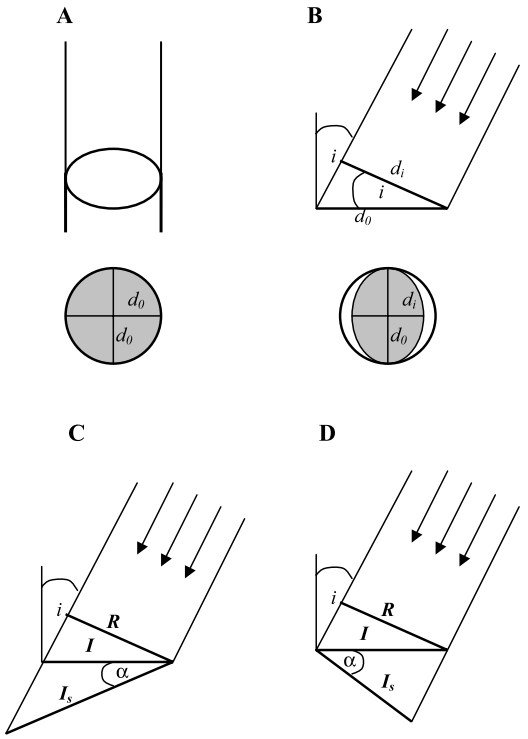

Figure 2. The effective receiving area of a rain gauge relative to incoming rainfall: (A) when $i = 0$; (B) when $i \neq 0$. The effective rain intensity at the soil surface of a sloping surface with aspect leeward from wind direction (C) and windward from wind direction (D). Symbols: d_0, diameter (m) of interception area when rain is falling vertical; d_i, diameter (m) of interception area when rain is falling under angle i (deg), R, intensity of rainfall with respect to a plane normal to the storm vector (m h^{-1}); I, intensity of rainfall measured with a horizontally placed gauge (m h^{-1}); I_s, rain intensity at the soil surface (m h^{-1}); α, slope (deg).

several studies there are still real difficulties in predicting the behaviour of crusts, and in particularly their effect on infiltration and overland flow. The mechanisms involved in the formation of the soil crust and the interactive effects of hydrological processes, the wind erosion processes and the development of a soil crust are not yet fully understood, especially in terms of the changes in the pore structure and hence hydraulic properties with time.

The generally sandy Sahelian soils are prone to crusting. Five main crust types can be identified: the structural crust, the erosion crust, the coarse pavement crust, the runoff and the still depositional crust (Valentin and Bresson, 1992). The coarse pavement crust is generally only found on degraded zones whereas all other crust types can also be found within cultivated fields. A structural crust typically consists of two layers. At a depth of a few millimetres a plasmic layer is formed by the clay and silt particles that are washed out from the top layer by raindrops. This plasmic layer is covered by loose cohesionless sand, which can easily be transported by wind or water. When this loose layer is removed and the plasmic layer is exposed, the crust is called an erosion crust. The coarse pavement crust resembles the structural crust in that it has two layers, with one being a generally more developed plasmic layer. This layer is overlain by coarse fragments which are partly embedded in the plasmic layer. The still depositional crust develops in standing water and is characterized by a vertical particle size distribution with coarse particles at the bottom and the finer particles at the top. When this crust dries up, it often breaks up into curled-up plates. Runoff depositional crusts develop in flowing water and are characterized by a microbedded layer (Boiffin and Bresson, 1987). Runoff and disjunction between fine and coarse particles induce alternating sub-millimetre microbeds, which are more or less contrasted in texture and unconformable with the underlying soil. This type of crust is often overlain by a structural crust.

A two- or three-layered Green and Ampt approach to simulate infiltration into the crusted soil would be a straightforward approach. However, using this approach, detailed information about the crust thickness and the hydraulic conductivity of the crust and the undisturbed soil underneath is needed. These parameters are already difficult to determine in the laboratory, but in the field this becomes an infeasible operation. Therefore here a one-layered Green

and Ampt model is employed using an effective hydraulic conductivity K_e (cm s^{-1}), which is a combination of the hydraulic conductivity of the undisturbed soil and that of the soil crust and has to be measured in the field.

Prior to ponding ($t < t_p$), rainfall intensity is less than the potential infiltration rate. In this period infiltration rate f is equal to the rain intensity I_s. Cumulative infiltration is calculated as:

$$F_t = F_{t-1} + I_s \Delta t \tag{5}$$

where F_t is the cumulative infiltration at the current time step (cm), F_{t-1} is the cumulative infiltration at the previous time step (cm), I_s is rain intensity at the soil surface (cm h^{-1}) and Δt is the duration of the time step (h).

Ponding begins when the rainfall intensity exceeds the potential infiltration rate ($t = t_p$). As rainfall continues ($t > t_p$), the saturated zone extends deeper into the soil and overland flow occurs from the ponded water. After ponding the cumulative infiltration is (Chow *et al*., 1988):

$$F_t = F_{t-1} + K_e \Delta t + \psi \Delta\theta \ln\left[\frac{F_t + \psi\Delta\theta}{F_{t-1} + \psi\Delta\theta}\right] \tag{6}$$

Equation 7 is solved by the method of successive approximation to give F_t.

In the Green and Ampt equation the infiltration rate f (cm h^{-1}) and the cumulative infiltration F are related by (Chow *et al*., 1988):

$$f_t = K_e\left(\frac{\psi\Delta\theta}{F_t} + 1\right) \tag{7}$$

where ψ is the wetting front capillary pressure head, and $\Delta\theta$ is the difference between the initial and the final moisture contents of the soil.

Determination of ponding time under rainfall of variable intensity is done by the following approach (Chow *et al*., 1988). Cumulative infiltration is calculated from rainfall as a function of time using Equation 5. A potential infiltration rate can be calculated from the cumulative infiltration using the Green and Ampt infiltration equation (Equation 7). Whenever rainfall intensity is greater than the potential infiltration rate, ponding occurs, and for the next time step Equation 6 should be used for calculating the cumulative infiltration. When rain intensity drops again below the potential infiltration rate, Equation 5 is used again to calculate cumulative infiltration.

Overland flow

Due to the small differences in topography, concentration of flow hardly occurs and overland flow generally takes the form of sheet flow. Traditionally, the rill and inter-rill processes are modelled in such a way that detachment by flow occurs only in the rill area and splash erosion detachment occurs only in the inter-rill area.

Since rill erosion does not occur in the described research areas and to enhance model speed, the rill erosion formulas are not considered in this model. However, it is acknowledged that transport capacity of sheet flow will become higher due to the effect of rainfall. The following equation for the raindrop impact contribution to the transport capacity of sheet flow is used (Guy *et al*., 1987):

$$TC_r = 4{\cdot}909 \times 10^6 I_s^{2{\cdot}014} S^{0{\cdot}865} \tag{8}$$

where TC_r is additional transport capacity (kg m^{-1} s^{-1}), I_s is rainfall intensity (m s^{-1}), S is slope (m m^{-1}).

Total transport capacity of the sheet flow will be equal to transport capacity (TC) as calculated by EUROSEM (Equation VIII, Table I) plus the additional transport capacity (TC_r).

Deposition will occur when the sediment load becomes higher than the transport capacity. The rate of deposition is dependent on the distance the sediment has travelled and the settling velocity. The following equation is used to determine the settling velocity (Marshall and Holmes, 1979):

$$v_s = 2(\rho_s - \rho_w)g\frac{\sqrt{D50/2000000}}{9\upsilon_w} \tag{9}$$

where v_s is settling velocity (m s^{-1}), ρ_s is particle density (kg m^{-3}) ρ_w is density of water (kg m^{-3}), g is acceleration of gravity, $D50$ is median grain size (cm) and υ_w is the viscosity of water.

Pool formation

Due to the small height differences in the topography in the Sahelian zone of northern Burkina Faso, pool formation occurs, limiting overland flow discharge and causing resettlement of sediments. These pools generally have a depth of several centimetres, but may extend over several tens of metres. Infiltration in these pools is often low due to the development of a still depositional crust. Due to low infiltration capacity and the large surface, most of the water evaporates fast in the hours after the rainfall event.

The input parameters necessary for simulation of pool formation are calculated on the basis of information from a digital elevation model (DEM) of the terrain. Based on this DEM a local drain direction (LDD) map can be created. An LDD gives, for each cell, the stream direction of water flowing in that cell. Cells that do not border on lower situated cells form pits. Pits are cells without a flow direction. In the case of pool formation pits are created at the deepest point in the pool. The map with the location of the deepest points of the pools is an input map of the model.

For each pit its sub-catchment is determined. Then by using information from the DEM the height and position of the overflow points can be determined. The map with the locations of the overflow points is input for the model. Based on the height of the overflow point, the maximal extension and volume of the pools can be calculated, which are also input parameters. Finally the LDD should be adapted so that the water will be directed towards the outflow point instead of to the pool pit. This is achieved by adding the maximum height of water (m per cell size) to the DEM and calculating a new LDD based on the 'full' DEM. This LDD map will also be input to the model.

Simulation of pool formation is based on a method described by Van der Plank (2002) and simulated as follows. All the water that has reached the outflow point, plus the rain in the pool, plus the water already in the pool is directed to the pool pit, which results in a water tower in this cell. This water tower map is at all points equal to the original DEM (m) except at the pool pits, where all the available water (m) is added to the DEM (Figure 3A). If the water tower at the pit is higher than the maximal volume of water that can be stored in the pool, the remainder is directed to the outflow point and will be regarded as water added to the stream flow in the downstream cell.

The amount of water in the water tower should be spread over the pool area in order to be able to determine the water depth at each cell (for calculation of detachment). Since the pool bottom is not flat, it is not exactly known over which area the available water is spread. To determine the exact pool area the model starts with the assumption that the pool has its maximum extension (which is an input parameter in the model). The amount of water available in the water tower will be averaged over the pool area. This results in an area, which is partly lower than the original DEM (Figure 3B). The water mirror in the lower parts is actually lower than the water mirror should be since the higher areas of the DEM, which actually are outside the pool area, are included.

Because the water mirror cannot be lower than the height of the original DEM, the cut-line between the original DEM and the calculated water level can be seen as the new maximal extension of the pool. When mediation of the water over this smaller area is performed, the calculated area of the water level will become more precise (Figure 3C). Even now there will be an area lower than the original DEM, but this area will be substantially smaller than that after the first mediation. Theoretically, after each mediation the height of the water mirror and the maximum extension of the pool will become more precise, but the perfect height and extension will never be reached. However, the error will become smaller after each mediation and after a certain number of repetitions become nil and fall within the resolution of the raster (Figure 3D). After the water height in the pool is determined, infiltration occurs over the whole pool area. In the next time step new water can be added to the pool.

In nature the flow direction of water in and to a pool changes with pool development. At the onset of pool formation all water streams in the direction of the lowest point. As soon as the pool is full the flow direction changes towards the point where the pool overflows.

In order to avoid problems with working with several LDDs (starting with the original one directing water to the pool pits and ending with the 'full pool' LDD) it was decided to work only with the 'full pool' LDD. All water that reaches the outflow point of the pool is redirected to the pool pit until the maximum pool volume is reached. This solution works well for the water part of the model; however, for the sediment part another scenario has been developed. As soon as the overland flow reaches the pool area, the transport capacity will become zero and deposition will occur. However, since we do take the settlement velocity into account, not all sediment is deposited at the pool borders, but deposition will decline towards the outflow point.

This solution will create a small error in the area where the actual drain direction is opposite to the overall drain direction of the 'full pool' LDD. It is assumed that these slopes do not contribute much to the sediment budget of the pool since they will be covered with water in an early stage of the rainfall event. Detachment in this area will be greatly limited. Furthermore, these slopes do not have a large sediment-contributing area.

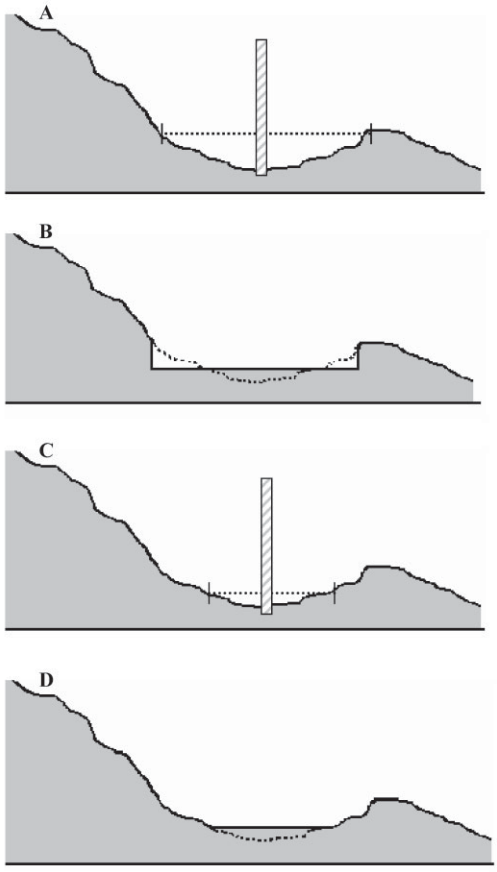

Figure 3. (A) Cross-section of the DEM at the pool pit with the available amount of water for pool formation. The dashed line indicates the area with the maximal pool extension. (B) Cross-section of the DEM after mediation of the available water with the maximal extension area of the pool. The dashed line indicates the original form of the DEM. (C) Cross-section of the DEM at the pool pit with the available amount of water for pool formation. The dashed line indicates the area where the pool will be calculated the second time. (D) Cross-section of the DEM after the pool area and water mirror have been calculated.

Research area

In the Sahelian zone of northern Burkina Faso, five main geomorphologic units can be distinguished. The gentle sloping pediplanes are interrupted by the smoothed ancient dune complexes, temporally flooded rivers, young dunes which might still be active, and by small hills (Zerbo, 1993). The hills are geological remnants, have a height of 100–200 m and cover only a small part of the country site. When stabilized, the young dunes are often cultivated. The young dunes generally have steep slopes and high infiltration capacities. The ephemeral rivers are deeply incised and carry water only during and shortly after heavy rainfall events. The rivers are often bordered by a band of dense vegetation up to 50 m from the riverbed. The area directly next to this band of vegetation is often cultivated. Approximately 90 per cent of the ancient dunes is cultivated and the pediplanes are generally used as grazing zones. At the ancient dunes, the areas next to the rivers and at the pediplane slopes are generally low (0–5°) and runoff mostly occurs in the form of sheet flow. Due to the small height differences, pool formation occurs, limiting runoff discharge and causing resettlement of sediment.

The Katchari catchment is situated in the Seno province in northern Burkina Faso (14°00″, 0°00″ W), 11 km west of Dori, the province capital. The climate is characterized by a short rainy season of 3–4 months starting in May–June. The mean annual precipitation is approximately 480 mm, but can be highly variable from year to year. Generally the first rains come from the east. Over the season rainfall depth and occurrence can be highly variable as seen in Figure 4A and B. Temperatures are high all year round, but two hot periods can be distinguished: the first starts in April and lasts till the beginning of the rainy season; the second immediately follows the rainy season (September) and lasts till the onset of the Harmattan winds in November–December.

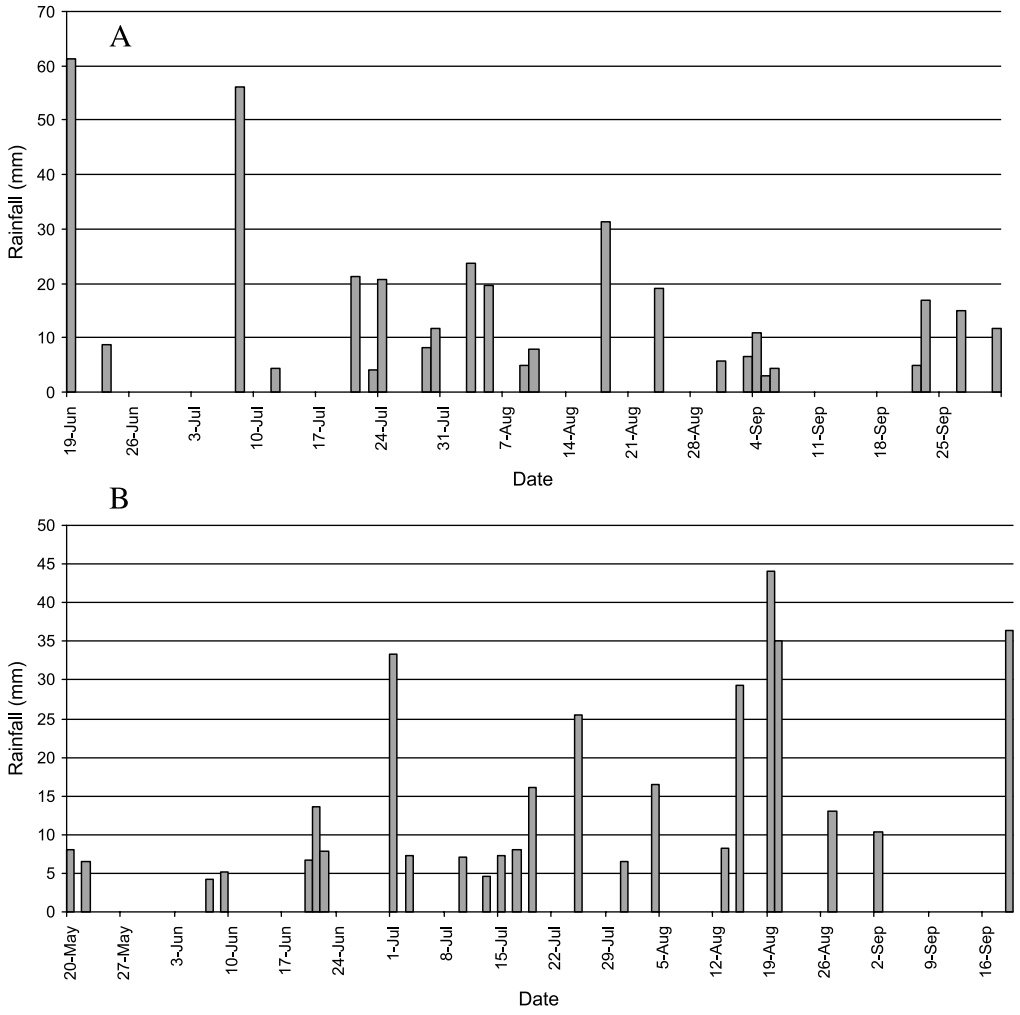

Figure 4. Rainfall at the degraded site in the Katchari catchment for the years 2000 (A) and 2001 (B).

Measurements were performed at three different geomorphologic settings: a degraded site, a cultivated field next to the ephemeral river (from now on referred to as valley), and a field at an old dune complex. The degraded site is characterized by its lack of vegetation and a well-developed coarse pavement crust, which covers approximately 75 per cent of the research plot. The coarse pavement crust consists of a well-developed erosion crust, with gravel embedded and overlain by loose gravel with coverage of 30–70 per cent. An erosion crust with significantly less embedded gravel covers the other 25 per cent of the research plot. The research site at the valley floor is cultivated with millet in the wet season and characterized by the fast development of erosion and still depositional crusts (Valentin and Bresson, 1992). Natural vegetation (trees and herbs) is scattered over the field. Annual herbs are removed by hoeing twice in the wet season. At the south-central part of the research plot a still deposition crust had developed. At this part of the field no millet was sown nor was it tilled during the research period. The dune is part of an old and flattened dune band belonging to an extensive sand dune system, which is more than 40 000 years old (Courel, 1977). The loamy, sandy soils of this dune complex are prone to crusting, with structural and erosion crusts being the most common. At the dune natural vegetation is also present; however, trees and shrubs are used to demarcate fields. Within the cultivated fields trees are rarely found.

All fields are characterized by an undulating topography. Maximum height differences within the site of the dune were approximately 0·5 m. At the valley floor and the degraded site the distances between depressions and crests ranged from 10 to 40 m with maximum height differences of approximately 1 m.

Measurements

During the rainy season of 2000 and 2001 field data of water erosion events were collected at three sites in the Katchari catchment. The degraded site and the dune site were equipped with a complete weather station continuously measuring average wind speed and direction, average temperature, and total rainfall at 1-min intervals. Average soil moisture content and total solar energy were continuously measured at 5-min intervals. Since the research site at the valley was situated less than 500 m from the degraded site, weather data from the degraded site were used for the valley during the 2000 rainy season. During the 2001 rainy season the valley site was equipped with an automatic rain gauge, which measured rainfall amounts at 1-min intervals.

At each site three runoff plots were installed, one with an area of 1 m^2 (1 × 1 m) and two with an area of 20 m^2 (10 m long, 2 m wide). Each plot was closed at its upper boundary so that run-on was not possible. The positions of the plots in the research site were chosen so that they were representative of the whole site with regard to the slope, crop coverage and crust type.

Under the 1-m^2 plots an automatic tipping bucket was installed, which recorded overland flow intensity at 1-min intervals. These measurements were used to compare measured time to ponding and peak discharge of overland flow with model predictions of these variables. Time to ponding is defined as the moment of first measurement of overland flow. Furthermore, total measured overland flow at the 1-m^2 plots was compared with the model predictions. The field measurements at the 1-m^2 plots were used to calibrate the model.

Overland flow and sediment load from the 20-m^2 plots were captured in four oil barrels at the end of the plot. The oil barrels could trap a maximum of 600 litres of water, which was similar to 30 mm of overland flow. After a rainfall event the total collected overland flow was measured with a precision of 0·5 l. All water and sediment of the first two oil barrels was deposed into two large buckets and left for 48 hours so that resettlement of sediment in suspension could occur. After this time period the water was poured and the sediment was collected, sun-dried for at least 5 hours and weighted. These measurements were used to compare measured total overland flow and total sediment load with model predictions.

The types of crust found in the field are usually related to topography and surface hydrology (Philibert, 2000; Valentin and Bresson, 1992). So, to get an impression of the flow direction and areas of erosion and deposition in the research sites, descriptions of crust development on the research plots were made during the 2001 rainy season. After each event crust development was described for two transects (one from NE to SW and one from NW to SE) and the topography of transects was measured with a level, four times during the rainy season. Comparing crust development with the model predictions of positions of erosion and deposition in the field could give an indication of the precision of the model. Furthermore, the positions of pool formation could be identified by the occurrence of a still deposition crust and compared with the position of pools based on the DEM.

Input values for the effective hydrologic conductivity (K_e) were based on the work of Horstman (2003) who measured the effect of crust development on infiltration characteristics with a disc-infiltrometer in the Katchari catchment. Infiltration values just after ploughing were based on the literature (Chow *et al*., 1988). Since K_e is related to crust type, a non-uniform distribution of the K_e input value over a uniform land use unit is obtained as an input parameter of the model.

The detachability of the soil by raindrop impact (k, Table II) is expressed as the weight of soil particles per unit of rainfall energy (g J^{-1}). It is measured in the field with splash cups (Poesen, 1985), and corrected for the effect of cup size (Poesen and Torri, 1988). Since crust development causes further compaction of the topsoil, more energy will be needed to detach the same amount of soil once a crust is formed. The measurement of soil detachability with splash cups should be performed on bare soil (Morgan *et al*., 1992). After consulting the owner of the fields in the valley and dune, it was agreed that part of the field could be left uncultivated to be able to perform measurements with splash cups. Though this allowed us to perform measurements during the time, it did not allow us to measure at the various crust types. So soil detachability at one moment in time was taken as uniform for the whole research site, which could lead to errors in model prediction.

Results and Discussion

In the 2000 rainy season rainfall started on 19 June with a large event of 62 mm within 2·5 hours (Figure 4A). This event was followed by a dry period of 4 weeks, which forced the farmers to re-sow their fields. The third rainfall event on 8 July was once again a large event, this time of 54 mm. Total rainfall in the 2000 rainy season was 382 mm.

In 2001, first rains fell in May, but since these were only small events and early in the season, farmers did not start to sow their fields until after the rains of 10 July. First and second cultivation occurred on 24 July and 18 August at the dune site and on 30 July and 30 August at the valley site. Total rainfall in the 2001 rainy season was 360 mm.

Table III. Measured and predicted runoff amounts on 1-m^2 plots during the 2001 rainy season. Plots were located at three geomorphologic units in the Katchari catchment, Burkina Faso

	Valley				Dune				Degraded site			
Date	***P* (mm)**	***D* (min)**	**R_m (mm)**	**R_p (mm)**	***P* (mm)**	***D* (min)**	**R_m (mm)**	**R_p (mm)**	***P* (mm)**	***D* (min)**	**R_m (mm)**	**R_p (mm)**
21 June	13·2	45	3·8	3·8	13·3	46	–	4·2	13·1	48	10·3	6·1
2 July	17·4	76	–	5·1	30·1	94	–	17·2	30·2	95	–	19·9
25 July	23·5	186	8·1	9·1	23·5	215	6·4	6·2	23·2	215	8·1	11·2
4 Aug	10·5	202	0·0	0·0	11·7	48	0·0	0·0	11·5	49	3·4	4·2
14 Aug	4·9	13	2·2	3·2	6·9	11	2·0	2·3	16·8	11	–	4·7
15 Aug	26·2	194	9·9	9·1	28·6	230	15·4	11·0	28·6	230	15·8	16·2
19 Aug	16·6	193	17·4	16·0	29·3	191	6·9	6·3	43·0	198	–	25·9
20 Aug	34·0	65	26·2	22·8	27·6	62	13·8	13·8	33·8	67	–	24·6
27 Aug	13·0	24	–	7·3	9·5	23	–	3·1	11·8	25	6·4	7·0
2 Sept	9·2	214	–	0·0	8·6	251	–	0·0	8·5	76	2·1	3·5
19 Sept	23·2	250	–	0·15	21·8	198	7·4	4·2	34·6	255	–	17·5

P, rainfall; *D*, duration; R_m, measured overland flow; R_s, predicted overland flow; –, no measurements made

Due to malfunction of equipment in the 2000 rainy season, a more complete and extended data set was available for the 2001 rainy season. Therefore, it was decided to calibrate and run the model for 11 events of the 2001 rainy season. Table III shows the total amounts of precipitation and duration of the selected events for each geomorphologic unit. Table III also shows that although rainfall amounts at the valley site and the degraded site are comparable for many events, the assumption that rainfall data from the degraded site could be used for the valley site is not justified. Care was taken to select events that were representative for all events that occurred in 2000 and 2001 both for total amount of rainfall and duration of the event.

Rainfall and overland flow were simulated for all events at three different scales: small runoff plots (1 m^2), large runoff plots (20 m^2) and research plot (6400 m^2). For simulation at the scale of both types of runoff plots pool formation was not considered, as the surfaces of these plots were relatively homogeneous, and without major depressions.

Model calibration at 1-m^2 runoff plots

The model was calibrated by varying the effective hydrologic conductivity (K_e) for each site and each crust type. Table III gives an overview of the final input parameters for K_e for the each crust type.

Horstman (2003) showed that the effective hydrologic conductivity changes over time due to cultivation practices and crust development. Therefore this value changes over the season. Furthermore, Horstman (2003) found that the infiltration characteristics of the well-developed erosion and coarse pavement crusts at the degraded site and the still depositional crust at the valley (which had not been cultivated for 4 years) showed no decrease in infiltration capacity through time. For these crust types, once calibrated, the K_e values were taken as constant over the season (Table IV). It was decided to use constant K_e values for the erosion crust at the valley and the dune. Since the erosion crusts at the valley and the dune were less developed than the erosion crust at the degraded site, these values were significant higher (Table IV). The transition from erosion to structural crust occurs gradually. It is possible to find both erosion and structural crusts within 1 m^2 (the size of a pixel). Rainfall simulations and disc-infiltrometer measurements showed that the effective hydrologic conductivity for these kinds of surfaces is significantly lower than that of the structural crust alone but higher than that of the erosion crust (Horstman, 2003) (Table IV). However, over the season, no significant decrease in K_e for these kinds of surfaces was found, therefore the input value was constant over the season.

Figure 5 shows the correlations between measured and simulated overland flow for the three geomorphologic units after calibration. Correlation was best for the valley and, though still acceptable, the degraded site showed the weakest correlation. Table III shows total amounts of measured and simulated overland flow for the 1 m^2 plots at the three research sites. For the valley and the dune sites, total overland flow was generally slightly underestimated, whereas for the degraded site a general overestimation occurred. Deviation of the simulated overland flow was generally around 5–8 per cent from the measured overland flow, with the exception of the event on 15 August at the dune, which resulted in an underestimation of 28·5 per cent at the dune.

Table IV. Model input values of the effective infiltration capacity (K_e) of various crust types at the degraded site, the dune and the valley in the Katchari catchment, Burkina Faso. The range values for the structural crust indicates the highest and lowest values used, with the highest values used after the first rain after ploughing

Site	Crust type	K_e (cm h^{-1})
Degraded site	Gravel crust	0·15
	Erosion crust	0·09
Vally site	Still depositional crust	0·15
	Just ploughed	1·1
	Structural	0·43–0·61
	Erosion	0·25
	50% structural, 50% erosion	0·28
Dune site	Just ploughed	2·9
	Structural	0·34–0·50
	Erosion	0·19
	50% structural, 50 erosion	0·26

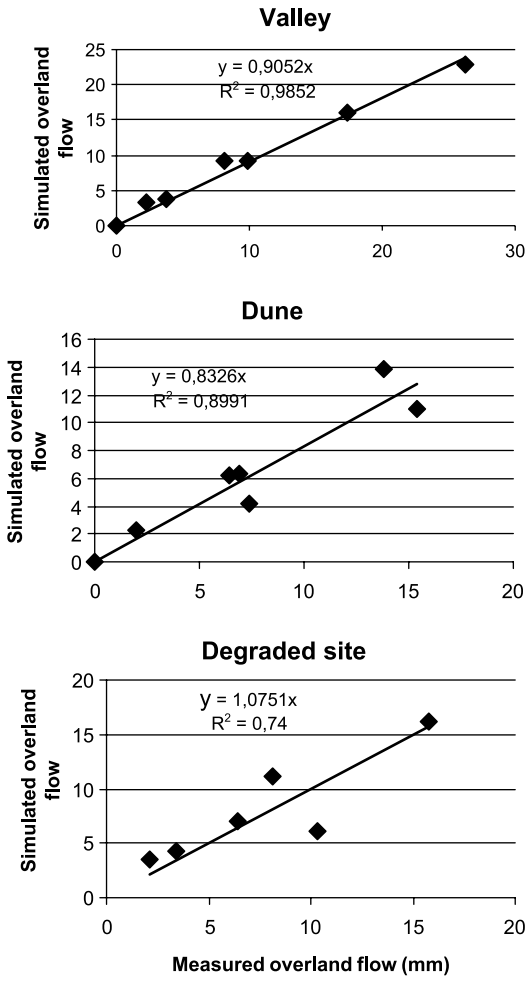

Figure 5. Correlation between measured and simulated overland flow at the valley, the dune and the degraded site in the Katchari catchment, northern Burkina Faso.

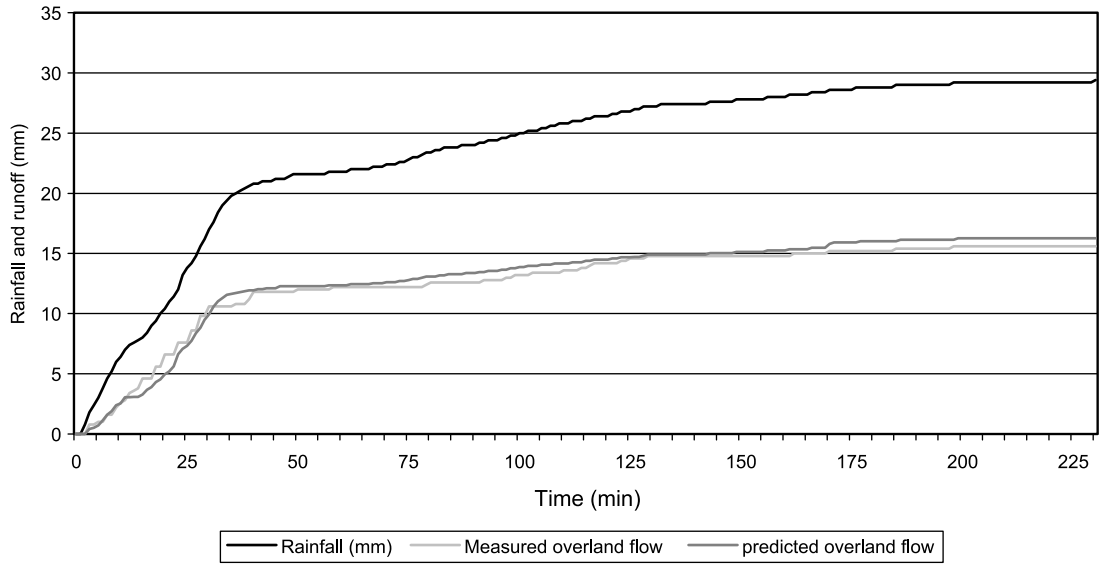

Figure 6. Cumulative rainfall and cumulative measured and simulated overland flow for a water erosion event on 15 August 2001 at the degraded site.

Comparison of model predictions of time to ponding and overland flow discharge with the measured values, generally showed a good agreement (Figure 6). For the degraded site simulated ponding generally occurred in the same minute as the first measured overland flow. At both the valley and dune sites a deviation of 1–2 min between simulated and measured time to ponding occurred. This deviation could be caused by the model simplification at this scale. Due to the small plot size it is assumed that all water that does not infiltrate in one time step leaves the simulation area. So no routing with the kinematic wave, as for the larger plot sizes, is simulated. Especially at the plots of the valley and the dune, where slopes were lower than those of the degraded site, this assumption may lead to small errors in the moment the overland flow reaches the plot outlet.

Large runoff plot model simulation

Table V shows the measured and simulated total overland flow and total sediment discharges for the 20 m^2 runoff plots at the three research sites. At the installation of the runoff plots care was taken that the two plots were equal in vegetation/crop cover, slope, and crust cover and could be considered as replicas. Therefore the measured values for the overland flow and sediment load are the average values of measurements at the two runoff plots. For all simulations at all sites more sediment was detached than transported. For example for the event of 21 June at the degraded site, total detachment (splash detachment + flow detachment) was 17·8 kg, and total deposition was 17·5 kg, resulting in a total soil loss over a 20 m^2 area of 0·3 kg. Furthermore, sediment fluxes (g m^{-3} s^{-1}) were equal to transport capacity (g m^{-3} s^{-1}) indicating that sediment transport was transport capacity limited. The transport capacity is low due to the low slopes and the fact that here we deal with sheet flow. Most of the detached sediment was directly deposed within the same cell. This indicates that splash detachment was the most important sediment-detaching process.

At the degraded site overland flow was generally well predicted. Sediment discharge was well predicted for five out of the eight events for which the sediment discharge was measured. At the dune site simulated overland flow was generally of the same order of magnitude as the measured overland flow. However, for all simulations overland flow was slightly overestimated. Ants were active at parts of the runoff plots at the dune. Ants rework the soil and break up crusts causing larger infiltration capacities (Mando, 1997). At the valley site overland flow was well predicted for 8 out of 11 events and sediment discharge was correctly estimated for 4 out of 7 events. At the dune site sediment discharge was correctly estimated for 3 out of 5 events. For all sites, when sediment discharge was not well predicted it was underestimated.

A possible explanation for the underestimation of sediment discharge can be found in the calculation of the transport capacity, especially in the effect of rainfall on the transport capacity. In calculating the effect of wind-driven rainfall on the inter-rill transport capacity, Guy *et al*. (1987) assumed vertically falling rainfall. Wind-driven rainfall

Table V. Measured (R_m) and predicted (R_p) overland flow and sediment discharge (S) for the 20-m^2 runoff plots at three geomorphologic zones in the Katchari catchment, 2001 rainy season

	Valley				Dune				Degraded site			
Date	R_m (mm)	R_p (mm)	S_m (kg)	S_p (kg)	R_m (mm)	R_p (mm)	S_m (kg)	S_p (kg)	R_m (mm)	R_p (mm)	S_m (kg)	S_p (kg)
21 June	3·5	5·4	0·9	0·2	0·4	2·3	–	0·1	3·9	5·8	–	0·3
2 July	10·1	7·7	–	0·3	11·7	18·6	1·3	1·2	21·4	21·2	5·6	2·1
25 July	13·5	10·1	0·8	0·4	0·4	0·5	0·0	0·0	23·7	9·9	3·2	0·5
4 Aug	0·1	0·0	–	0·0	0·1	0·0	–	0·0	5·9	4·6	–	0·2
14 Aug	0·2	0·9	–	0·0	0·0	0·6	–	0·1	4·1	4·4	–	0·4
15 Aug	2·9	6·9	0·6	0·2	10·3	9·8	0·7	0·2	18·2	14·7	1·9	0·7
19 Aug	11·3	11·3	1·7	0·3	1·0	2·0	0·6	0·1	26·6	25·8	1·5	1·8
20 Aug	24·2	22·8	1·8	1·6	8·3	12·7	0·4	0·7	24·2	25·7	1·5	2·1
27 Aug	1·5	0·9	0·2	0·1	0·1	2·5	–	0·1	6·3	7·5	1·4	1·1
2 Sept	0·0	0·1	0	0·0	0	0·0	–	0·0	0·1	0·0	0·1	0·0
19 Sept	2·3	4·4	0·2	0·0	0·1	0·0	–	0·0	12·8	15·4	0·8	0·6

exerts a larger kinetic energy on the soil surface (Pedersen and Hasholt, 1995) and so also on the water layer. This additional energy creates more turbulence. So the transport capacity of sheet flow under wind-driven rain might be larger than that of sheet flow under vertically falling rain with the same intensity. The fact that sediment discharge is underestimated more at the valley and the dune than at the degraded site can be explained by the differences in slope. At the degraded site the slopes are generally larger and so the stream velocity of the sheet flow is also larger, resulting in larger transport capacities. Probably transport capacity of inter-rill flow is only significantly affected by wind-driven rain when slopes are very low (0–2°). The large underestimation of sediment discharge for the event of 25 July at the degraded site can be explained by the fact that wind-blown sediment transport occurred during 7 min preceding rainfall. It is possible that the gutter of the runoff plot trapped some sediment and that sediment entered the oil barrels through small holes between the cover and the barrel. This led to an overestimation of sediment discharge.

Overland flow for the event of 25 July is also highly underestimated for the degraded site and the valley site (the dune site had just been cultivated so much water could infiltrate). This is most probably due to the character of rainfall; during the first 20 min there was a total of 14·6 mm of rainfall with an intensity up to 78 mm h^{-1} followed by three hours of drizzle totalling 9·8 mm. When measuring drizzle with a tipping bucket rain gauge, instead of recording continuous rainfall, it appears that is does not rain for 5 min, for example, followed by a minute of rainfall with an intensity of 12 mm h^{-1}.

The reason why this large underestimation of overland flow did not show while modelling at a smaller scale lies in the overland flow routing. Whereas overland flow at the small plots is simulated as reaching the outlet within one time step, this does not occur at the larger plots. When rainfall in one time step falls at the upper part of the plot and does not directly infiltrate, it takes, especially with the low slopes, at least one or two time steps (of 2 s) to reach the outlet. During these time steps the flowing water has the opportunity to infiltrate, which will occur especially when no rain is added. If a continuous, lower intensity rainfall had been input to the model, more overland flow would be simulated. A site with low infiltration capacities such as the degraded site is especially vulnerable for distribution of rainfall input. As can be seen in Table V for the valley site, this site is less vulnerable for the effects of drizzle, most probably due to the larger infiltration capacities. Still an underestimation of overland flow occurred.

Research plot model simulation

As can be seen in Figure 7, pool formation is well simulated by the model. Pool formation starts at the deepest point in the pool (Figure 7A), continues until this point is completely filled up and starts to expand as rainfall continues (Figure 7B). With decreasing rainfall and continuing infiltration, pool size decreases again (Figure 7C). As can be concluded from Figure 7, pool formation does limit overland flow and, in this case, increase infiltration. If the development of a still depositional crust had been simulated in the model, pool extension would not decline so fast after the rainfall event. Now the standing pool water is allowed to infiltrate with an infiltration rate equal to that of the crust type the was present before the onset of the rainfall event, which was not always a still depositional crust. Furthermore, if the development of a still deposition crust were simulated during the event, less water would infiltrate in the pool area, resulting in an increased runoff.

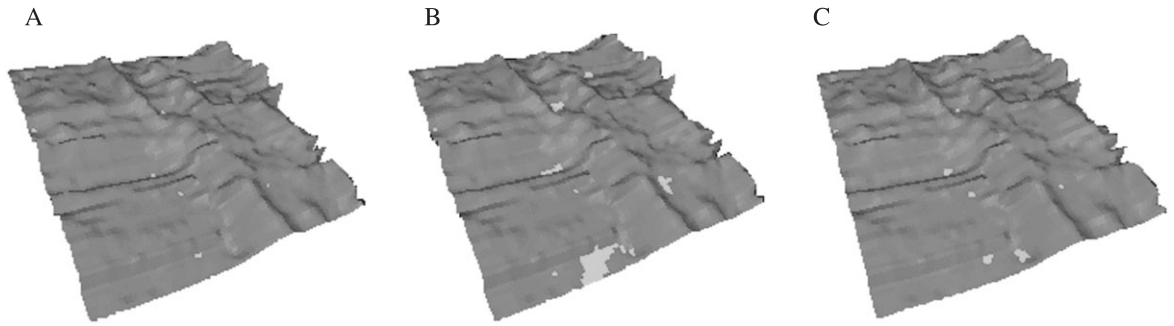

Figure 7. Extension of pools for the rainfall event of 14 August at the valley at 3 min (A), 13 min (B) and 25 min (C) after onset of rainfall. The clear areas indicate the extension of the pool.

Table VI. Soil loss from the simulation area at three geomorphologic zones in the Katchari catchment, 2001 rainy season

	Soil loss (kg ha^{-1})		
Date	**Valley site**	**Dune site**	**Degraded site**
21 June	7·4	6·2	16·6
2 July	10·9	66·7	55·8
25 July	1·6	0·4	183·4
4 Aug	1·0	0·0	57·1
14 Aug	0·1	1·5	2·6
15 Aug	6·4	15·3	310·2
19 Aug	393·9	4·5	580·4
20 Aug	46·6	50·4	872·4
27 Aug	0·1	4·1	47·5
2 Sept	0·0	0·0	0·0
19 Sept	0·8	0·1	251·3

The total simulation area of the valley and the degraded site was 6400 m^2 and the simulation area of the dune was 5226 m^2

Table VI shows for each event the total simulated soil losses from the three geomorphologic zones. Except for the event of 2 July, soil losses were highest at the degraded site. The generally low infiltration capacities at the degraded site cause large amounts of overland flow. From simulation at the scale of the runoff plots it was already clear that sediment transport was transport capacity limited. So more overland flow results in more soil loss since the sediment is available.

For the event of 2 July the highest soil losses were measured at the dune site. At this moment 80 per cent of the soil at the dune was covered with an erosion crust with a low infiltration capacity. The amount of rainfall was almost equal to the amount of rainfall at the degraded site, 30 mm (Table IV), whereas the valley only received 17 mm. Due to the finer texture of the soil at the dune (*d50* dune 0·0079 cm, *d50* degraded site 0·0151 cm), and despite the slightly lower total discharge, more sediment could be transported at the dune than at the degraded site.

Apart from the events of 2 July and 19 August, soil losses at the valley and the dune sites were generally in the same order of magnitude. Just before the event of 19 August the dune site was cultivated, crusts were removed and the infiltration capacity of the soil became high. Clearly less runoff occurred at the dune and soil loss was limited.

Comparing total soil loss (kg ha^{-1}) predicted for the plot scale with the predicted soil losses at the runoff plots (kg ha^{-1}), we see that predicted soil losses at the runoff plots are higher than predicted soil losses at the plot scale. For instance, predicted soil losses at the scale of a runoff plot for the well predicted event of 20 August were 755 kg ha^{-1} for the valley, 345 kg ha^{-1} for the dune and 1050 kg ha^{-1} for the degraded site. For the site scale simulated losses were 46·6 kg ha^{-1} at the valley, 50·4 kg ha^{-1} at the dune and 872·4 kg ha^{-1} at the degraded site (Tables IV and VI). This difference is partly explained by the fact that at the runoff plots no sediment-loaded water enters the plot. The overland flow in the upstream cells is loaded with sediment until maximum transport capacity is reached. This causes

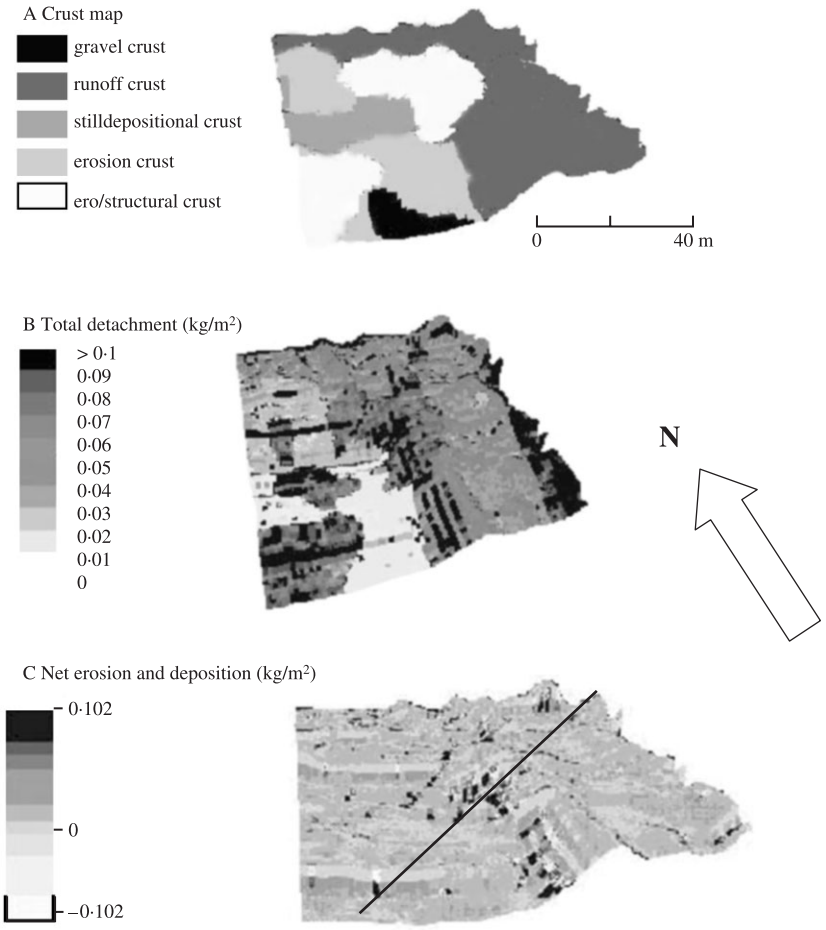

Figure 8. (A) Distribution of crust types at the valley before the event of 14 August. (B) Total detachment (kg m^2) during the event of 14 August 2001. (C) Net erosion and deposition after the event of 14 August at the valley. Positive numbers indicate deposition and negative numbers indicate erosion. The black line indicates the position of the transect of Figure 9.

more erosion in those particular cells than would have occurred if the water streaming into those cells had had a sediment load. Furthermore, resettlement occurs in areas with smoother slopes, resulting in lower total soil losses at the scale of the research plots.

Figure 8B shows total detachment (kg m^{-2}) for the event of 14 August at the valley. Comparing this map with the crust map (Figure 8A) it is clear that detachment is highly controlled by the crusting pattern. This goes for all events at the valley. Apparently raindrop detachment is the most important process; but on the somewhat steeper slopes additional detachment by flow occurs. Comparing Figure 8B with the net erosion and deposition map (kg m^{-2}) (Figure 8C), it becomes immediately clear that sediment transport is transport capacity limited. Almost all detached sediment is directly deposited, resulting in only small amounts of erosion.

When comparing the net erosion and deposition map with the crust-transect (Figure 9), we find that at the locations where the net effect is almost zero and where pool formation is simulated, a still depositional crust is formed. In the slightly steeper areas, where most erosion occurs, a runoff crust is formed, and in the areas where alternating smaller amounts of erosion and deposition occur, a mixture of structural and erosion crusts had developed. Due to the close relation of crust development with erosion and deposition (Philibert, 2000) we can conclude that the model gives reasonable results regarding the spatial distribution of erosion and deposition.

The previously mentioned conclusion, that sediment transport at the valley is transport capacity limited, also accounts for both the dune site and the degraded site. The large amounts of sediment that were detached by raindrop impact remain behind as loose particles available for transport by a future wind erosion event; these regularly develop in this area in the early rainy season (Sterk, 1997). In the literature a wide variety of references giving negative

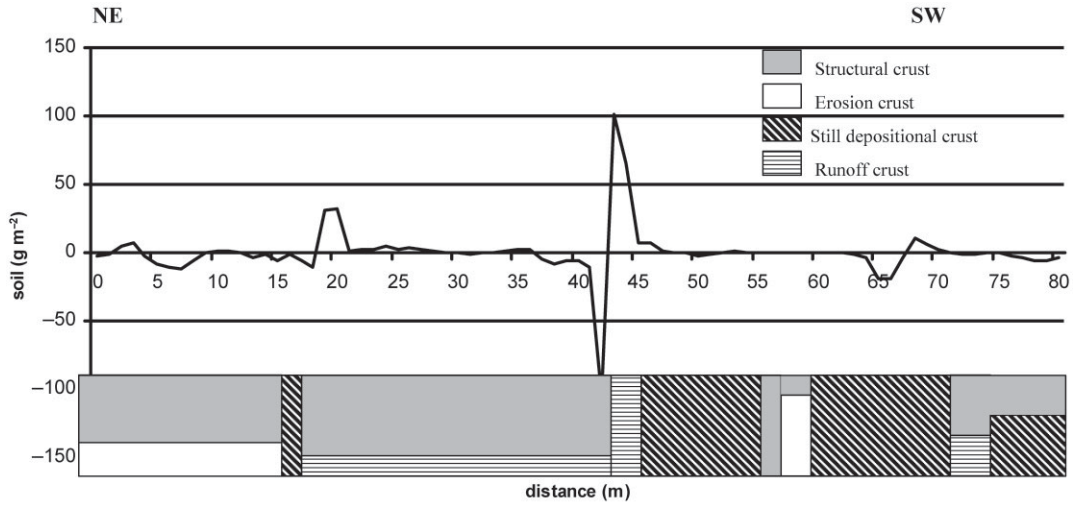

Figure 9. Erosion and deposition (g m^{-2}) versus crust type at the valley over a NE–SW transect after the event of 14 August 2001. The transect is measured along the white line from Figure 8. When two crust types occur at the same place, it indicates that both crust types occur side by side. Negative values indicate erosion and positive values indicate deposition.

sediment balances for farmers, fields in these areas can be found (Albergel *et al*., 2000; Collinet and Valentin, 1985; Joly *et al*., 1991). However, taking into account the low erosion rates found (Table VI), it has to be concluded that, in the current research area, it is not water erosion alone, but rather the interaction between wind and water erosion that causes these large negative balances. In this interaction water erosion is seen as the sediment delivery process, whereas wind erosion is the transporting process. This conclusion is also confirmed by the description of the crusts over time. Whereas in the early rainy season erosion crust covers the largest part of the field, later in the season the largest parts of the field are covered by the structural and runoff crusts. The fact that soil crusting has such a large influence on soil erosion by water, both in detachment and infiltration, implies that model performance in the Sahel could be improved by including crust development during the event, as was already stated by Valentin (1995).

Conclusion

The modified version of EUROSEM for the Sahel is a fully dynamic erosion model, able to simulate infiltration, overland flow routing, pool formation, sediment transport, and erosion and deposition by inter-rill processes over the land surface in individual storms at the scale of both runoff plots and fields. After calibration a good agreement between measured and simulated overland flow was obtained for simulation at 1 m^2 plots. Furthermore, time to ponding and overland flow discharge was predicted well by the model.

At the scale of a 20 m^2 runoff plot the model performed well and total measured and simulated overland flow were generally of the same order of magnitude for all sites. For all sites sediment transport was transport capacity limited. For several events the sediment discharge was underestimated. By incorporating the effect of wind-driven rain on transport capacity, this underestimation could most probably be avoided.

At the scale of the research site, the model performs well in the formation of pools, limiting total overland flow. However, due to the fact that development of a still depositional crust is not considered in the model, pool water infiltrates, which was not observed in the field.

The model simulates large amounts of detachment directly followed by deposition, suggesting that transport is transport capacity limited. However, the large amounts of detached sediment remain behind as loose particles, available for transport by a future wind erosion event. Therefore it is concluded that in this area, it is not water erosion alone but rather the interaction between wind and water erosion that causes negative nutrient and sediment balances.

Clearly crust development has a large influence on soil erosion by water in the Sahel, both on infiltration and detachment. So far we are only working with crust-related input parameters, which are fixed during the event. However, during the event the largest part of crust development occurs. Therefore, incorporating crust development would probably greatly enhance model performance.

References

Albergel J, Diatta M, Pépin Y. 2000. Aménagement hydraulique et bocage dans le bassin arachidier du Sénegal. In *Actes du séminaire international: La jachère en Afrique tropicale: Rôles, aménagement, alternatives*, Floret C, Pontanier R (eds). Dakar, Sénégal.

Bennet JP. 1974. Concepts of mathematical modelling of sediment yield. *Water Resources Research* **10**: 485–492.

Boiffin J, Bresson LM. 1987. Dynamique de formation des croûtes superficielles: raport de l'analyse microscopique. In *Micromorphologie des sols*, Fedoroff N, Bresson LM, Courty MA (eds). AFES: Plaisir; 393–399.

Brandt CJ. 1989. The size distribution of throughfall drops under vegetation canopies. *Catena* **16**: 507–524.

Bristow KL, Smetten KRJ, Ross PJ. 1994. Water entry into sealing, crusting and hardsetting soils: A review and illustrative simulation study. In *Sealing, Crusting and Hardsetting Soils: Productivity and Conservation*, So HB, Smith GD, Raine SR, Schafer BM, Loch RJ (eds). Australian Society of Soil Science Inc.: Brisbane, Australia; 183–203.

Chow VT, Maidment D, Mays LW. 1988. *Applied Hydrology*. McGraw-Hill Book Co: Singapore.

Collinet J, Valentin C. 1985. Evaluation of factors influencing water erosion in West Africa using rainfall simulation. In *Challenges in African Hydrology and water Resources*. IAHS Publication 144: 451–461.

Courel MF. 1977. Étude géomorphique des dunes du Sahel; Niger Nord occidental et Haut-Volta Septentrional. *Géology*. Université de Paris: Paris, France.

De Jong K. 1997. PCRaster homepage; info, software and manuals. http://www.modelkinetix.com/modelmaker/ [12 May 2002]

Govers G. 1990. Empirical relationships on the transporting capacity of overland flow. *International Association of Hydrological Science* **189**: 45–63.

Guy BT, Dickinson WT, Rudra RP. 1987. The roles of rainfall and runoff in sediment transport capacity of interrill flow. *Transactions of ASAE* **30**(5): 1378–1387.

Hoogmoed WB, Stroosnijder L. 1984. Crust formation o sandy soils in the Sahel. *Soil Tillage Research* **4**: 5–23.

Horstman H. 2003. *The influence of crust formation on infiltration characteristics*. Publication 31. Wageningen University: Wageningen.

Joly F, DeWolf Y, Chevallier P. 1991. L'eau et les sols. In *Une espace sahélien: la Mare d'Oursi, Burkina Faso*, Claudel J, Grouzis M, Milleville P (eds). ORSTOM éditions: Paris.

Kirkby MJ. 1980. Modelling water erosion processes. In *Soil Erosion*. Kirkby MJ, Morgan RPC (eds). Wiley: Chichester; 183–216.

Kutilek M, Nielsen DR. 1994. *Soil Hydrology*. Catena-Verlag: Cremlingen-Destedt.

Lal R. 1988. Soil degradation and the future in sub-Saharan Africa. *Journal of Soil and Water Conservation* **43**(6): 444–451.

Mando A. 1997. The impact of termites and mulch on the water balance of crusted Sahelian soil. *Soil Technology* **11**: 121–138.

Marshall TJ, Holmes JW. 1979. *Soil Physics*. Cambridge University Press: Cambridge.

Merriam RA. 1973. Fog drip from artificial leaves in a fog wind tunnel. *Water Resources Research* **9**: 1591–1598.

Morgan RPC. 1995. *Soil Erosion and Conservation* (second edn). Longman: London.

Morgan RPC, Quinton JN, Rickson RJ. 1992. *EUROSEM Documentation Manual*. Silsoe College: Silsoe.

Pedersen HS, Hasholt B. 1995. Influence of wind speed on rainsplash erosion. *Catena* **24**: 39–54.

Philibert V. 2000. *Surface crusting and soil erosion in northern Burkina Faso*. Publication 50. Wageningen University: Wageningen.

Poesen J. 1985. An improved splash transport model. *Zeitschrift für Geomophologie* **29**: 193–211.

Poesen J, Torri D. 1988. The effect of cup size on splash detachment and transport measurements. Part I: Field measurements. *Catena Supplement* **12**: 113–126.

Saleh A. 1993. Soil roughness measurement: chain method. *Journal of Soil and Water Conservation* **48**(6): 527–529.

Sharon D. 1980. The distribution of hydrologically effective rainfall incident on sloping ground. *Journal of Hydrology* **46**: 165–188.

Sivakumar MVK, Wallance JS. 1991. Soil water balance in the Sudano-Sahelian zone: need, relevance and objectives of the workshop. In *Soil Water Balance in the Sudano-Sahelian Zone*, Sivakumar MVK, Wallance JS, Renard C, Giroux C (eds). IAHS Press, Institute of Hydrology: Wallingford; 3–10.

Smith RE, Goodrich DA, Quinton JN. 1995. Dynamic distributed simulation of watershed erosion: KINEROS II and EUROSEM. *Journal of Soil Water Conservation* **50**: 517–520.

Sterk G. 1997. *Wind erosion in the Sahelian zone of Niger: Processes, Models and Control Techniques*. Publication 151. Department of Erosion and Soil & Water Conservation, Wageningen University: Wageningen.

Sterk G. 2003. Causes, consequences and control of wind erosion in Sahelian Africa: A review. *Land Degradation & Development* **14**: 95–108.

Thiombiano L. 2000. *Etude de l'importance des facteurs édaphiques et pédopaysagiques dans le développement de la désertification en zone Sahélienne du Burkina Faso, Pédologie*. L'Université de Cocody: Abidjan.

Umback CR, Lembke WD. 1966. Effects of wind on falling water drops. *Transactions of ASAE* **9**(6): 805–808.

Valentin C. 1995. Sealing crusting and hardsetting soils in Sahelian agriculture. In *Sealing, Crusting and Hardsetting Soils: Productivity and Conservation*, So HB (ed.). Australian Society of Soil Sciences: Brisbane, Australia; 53–76.

Valentin C, Bresson LM. 1992. Morphology, genesis and classification of surface crusts in loamy and sandy soils. *Geoderma* **55**: 225–245.

Van der Perk M, Slavik O. 2003. Simulation of event-based and long-term spatial redistribution of Chernobyl-derived radiocaesium within catchments using geographical information system embedded models. *Hydrological Processes* **17**(5): 943–957.

Van der Plank J. 2002. *Het Dam Model*. Utrecht, The Netherlands.

Van Dijck S, Karssenberg D. 2000. EUROSEM in PCRaster. http://www.geog.uu.nl/pcraster/runoff/eurosem/ [12 April 2003]

Van Elewijck L. 1989. Influence of leaf drip and branch slope on stemflow amount. *British Geomorphological Research Group Symposium on Vegetation and Geomorphology*: Bristol, UK.

Veihe A. 2000. Sustainable farming practices: Ghanaian farmers' perceptions of erosion and their use of conservation measures. *Environmental Management* **25**: 393–402.

Veihe A, Rey J, Quinton JN, Strauss P, Sancho FM, Somarriba M. 2001. Modelling of event-based soil erosion in Costa Rica, Nicaragua and Mexico: evaluation of the EUROSEM model. *Catena* **44**(3): 187–203.

Woolhiser DA, Smith RE, Goldrich DC. 1990. *KINEROS, A Kinematic Runoff and Erosion Model*. US Department of Agriculture: Washington DC.

Zerbo L. 1993. *Charactèrisation des stations de réchèrches agronomiques*. Di, Katchari, Kouare 109. Institut d'études et de réchèrches agricoles (INERA): Ouagadougou.

